Walker, D., Lord, OT., Walter, MJ., & Clark, SM. (2009). X-ray absorption contrast images of binary chemical reactions. *Chemical Geology*, *260*(3-4), 211 - 220. https://doi.org/10.1016/j.chemgeo.2008.12.025

Elsevier Editorial System(tm) for Chemical Geology
Manuscript Draft

Manuscript Number:

Title: X-ray Absorption Contrast Images of Binary Chemical Reactions

Article Type: Research Article

Keywords: X-ray imaging;
absorption contrast;
eutectic composition;
diamond anvil cells

Corresponding Author: Dr David Walker,

Corresponding Author's Institution: Columbia U

First Author: David Walker

Order of Authors: David Walker; Oliver T Lord; Michael J Walter; Simon M Clark

Abstract: Low-divergence synchrotron-sourced X-rays enable a radiographic imaging scheme for full characterization of binary chemical reactions and characterization by type of more complex reactions, in situ, in diamond anvil cells (DAC). Spatially resolved reactants are induced to react by laser heating of their interface. The spatially intermediate products are observed through X-ray absorption contrast. Limits to the technique include the ability to maintain controlled experiment geometry during compression and the ability to resolve chemical differences between reactants and products by X-ray absorption. The ability to make in situ observations at experimental pressure and temperature obviates the problem with quenching techniques for capturing liquid compositions in experiments with dimensions smaller than the diffusion length during quenching time. Partially molten Fe-alloy systems, of poor quenchability, are examined at DAC pressures and temperatures for relevance to Earth's core constitution and evolution. Determinations of eutectic melting in Fe-FeS match known results. Of the probable light elements that may alloy with Fe in the Earth's liquid outer core, Fe-FeS experiments show only modest quenching problems, but C and Si alloy experiments are highly vulnerable to quenching artifacts. The observed reactivity of FeS, Fe3C, FeSi, and

FeO(OH) with Fe in DAC makes the observed non-reactivity between Fe and FeO more significant, reducing the probability that oxygen alone is the major alloy in Earth's molten outer core.

# X-ray Absorption Contrast Images of Binary Chemical Reactions

D. Walker[1], O.T. Lord[2], M.J. Walter[2], and S.M. Clark[3]
[1]Lamont-Doherty Earth Observatory, Columbia University, Palisades NY 10964, USA
[2]Department of Earth Sciences, University of Bristol, Bristol, BS81RJ, UK
[3]Advanced Light Source, Lawrence Berkeley National Laboratory, MS6R2100, 1 Cyclotron Road, and Department of Earth and Planetary Science, University of California, Berkeley CA 94720, USA.

Abstract

Low-divergence synchrotron-sourced X-rays enable a radiographic imaging scheme for full characterization of binary chemical reactions and characterization by type of more complex reactions, *in situ,* in diamond anvil cells (DAC). Spatially resolved reactants are induced to react by laser heating of their interface. The spatially intermediate products are observed through X-ray absorption contrast. Limits to the technique include the ability to maintain controlled experiment geometry during compression and the ability to resolve chemical differences between reactants and products by X-ray absorption. The ability to make *in situ* observations at experimental pressure and temperature obviates the problem with quenching techniques for capturing liquid compositions in experiments with dimensions smaller than the diffusion length during quenching time. Partially molten Fe-alloy systems, of poor quenchability, are examined at DAC pressures and temperatures for relevance to Earth's core constitution and evolution. Determinations of eutectic melting in Fe-FeS match known results. Of the probable light elements that may alloy with Fe in the Earth's liquid outer core, Fe-FeS experiments show only modest quenching problems, but C and Si alloy experiments are highly vulnerable to quenching artifacts. The observed reactivity of FeS, $Fe_3C$, FeSi, and FeO(OH) with Fe in DAC makes the observed non-reactivity between Fe and FeO more significant, reducing the probability that oxygen alone is the major alloy in Earth's molten outer core.

## 1. Introduction

Earth's molten outer core is known (Birch, 1952) to have light element(s) alloyed with Fe, the most probable candidates for which are S, C, O, Si, and H. Distressingly little is known about the high pressure saturation limits of these elements in molten Fe, the eutectic compositions and temperatures as a function of pressure, the eutectic saturating phase, or even whether the nature of first melting in the binary systems remains eutectic at pressures relevant to the core, 1-3 Mbar. Given the likelihood that the candidate elements will be present in combination in Earth's core (Poirier, 1994) rather than as one exclusive of the others, the melting relations of the core system are little better than conjectural. Present knowledge mostly constrains the melting points of pure phases, a few scattered alloys, and isolated eutectics at pressures of at most ~a megabar.

Walker (2005) suggested a strategy for improving our knowledge base of the phase relations of relevant binary systems in the DAC pressure range. We report pilot experiments that demonstrate the feasibility of laser heating the lateral contact between thin wafers of spatially resolved reactants to form a product at the interface – usually a first-melting liquid – in binary chemical systems. X-ray absorption imaging of the experiment during progressive laser heating of the interface can detect phase appearance, at measured temperature, the chemical topology of the reaction, and the chemical composition of the first liquids produced from paired reactants.

## 2.1 Experimental methods

Experiments were carried out in diamond anvil cells (DAC) on beam line 12.2.2, shown in Figure 1, of the Advanced Light Source, Lawrence Berkeley National Laboratory [Kunz et al., 2005]. This is a dedicated high-pressure beam line equipped with brightness preserving X-ray optics and a double-sided laser heating system [Caldwell et al., 2007]. Hard X-rays are generated by a 5.29T super-bend magnet. The X-rays are vertically collimated by a parabolic silicon mirror. One wavelength is selected using a pair of Si(111) crystals mounted in an APM Kohzu monochromator. A toroidal mirror focuses the monochromatic x-ray beam through the DAC containing the experiment to a $CdWO_4$ phosphor, which converts the X-rays to visible light that is collected by a lens and projected onto a CCD detector. The phosphor screen is located about 5 cm behind the DAC experiment, and the low divergence of the X-ray beam preserves the coherence of the radiographic image at this distance. At the phosphor the focused beam size is about 50μm vertical and 3mm horizontal, which is smaller than the vertical field of view required for this experiment. Therefore the toroidal mirror is scanned through a tilt of about 0.02 mrad during an exposure to illuminate a vertical field of about 250 μm.

The transmitted X-rays are converted into visible light using a $CdWO_4$ crystal supplied by Hilger Crystals. The $CdWO_4$ crystal absorbs the x-rays and emits a broad-band of visible light from about 330 nm to 540 nm [Gurvich et al., 1977]. Our crystal had a maximum emission at 520 nm. Light emitted from the crystal is collected by a 20x Mitutoyo M Plan Apo SL lens (numerical aperture = 0.42) and delivered to an Apogee Instruments Inc. Alta U series digital CCD camera that consists of a 512x512 array of

20μm x 20μm pixels. The CCD has a dynamic range of >83dB and a peak quantum efficiency at 590 nm.

Most data were collected at 15-20 keV, energies that are intermediate between the lowest energy (6 keV) supplied by the monochromator but which is insufficient to penetrate the DAC diamonds, and the highest energies available (35 keV) that are too penetrating to resolve by absorption contrast the DAC gasket from the hole for the experiment. At 15 keV the attenuation length in $CdWO_4$ is 14μm, which gives a theoretical spatial resolution of about 1μm at 10% MTF (Modulation Transfer Function) at the CCD [Stampanoni et al., 2002] and is well matched to the projected image size. Imperfections in the scintillator crystal, aberrations from the transfer optics and slight misalignments of the scintillator, optics, and detector will degrade the actual resolution somewhat from the theoretical value, although the small field of view required for this measurement limits these effects. The X-ray flux on beam line 12.2.2 at the experiment is about $6.4 \times 10^{10}$ photons per second at 15 keV with a stored current of 400mA. The diamond anvil cell contains two diamonds each of 2.5mm height, which means that the beam has to pass through 5mm of diamond yielding a transmission factor for 15keV x-rays of about 0.3. Taking account of diamond absorption, $\sim 1.9 \times 10^{10}$ photons per second are available for the experiment and these are spread over the $1.5 \times 10^5$ $\mu m^2$ focal spot giving about $1.3 \times 10^5$ x-ray photons per second per pixel. For 15 keV X-rays the transmission factor for a 20 μm thick sample of Fe is 0.41 and FeO is 0.59. For two adjacent pixels one detecting x-rays that have traveled through 20 μm of Fe and the other detecting X-rays that have travelled through 20 μm of FeO, there should be about $5 \times 10^4$ and $7.5 \times 10^4$ X-ray photons respectively. A $CdWO_4$ crystal produces about 225 visible

light photons per incident 15 keV x-ray photon and our optics collect about 3.5% of that light, giving about 4.0 x $10^5$ photons/s collected by the CCD detector in a pixel illuminated by light generated by X-rays that have traveled through Fe and 5.8 x $10^5$ ph/s for FeO. Taking account of the quantum efficiency of the detector this gives 1.63 x $10^5$ electrons/s being produced for Fe and 2.33 x $10^5$ electrons/s for the FeO. Average exposure times per pixel were on the order of 1 second so that the number of electrons produced for the FeO exceeds the 2x$10^5$ electron well depth of the CCD. We therefore placed a 6.5 μm thick copper foil in the incident x-ray beam. The Cu foil changes the number of electrons produced in the CCD to 1.1 x $10^5$ for Fe and 1.52 x $10^5$ for FeO. The current produced by the CCD is converted into a digital signal using a 16 bit ADC. ADC results in 3.2 x $10^4$ counts being recorded for the Fe, and 4.6 x $10^4$ counts being recorded for the FeO. This gives an edge step of about 1.4 x $10^4$ counts. Assuming Poisson statistics, we estimate an error in our signal of 0.5% which translates into a maximum precision in our estimates of composition of about 1.5% of the step height between Fe and FeO or 0.3 wt. % oxygen in FeO.

The laser heating system consists of two 100 W cw fiber lasers (SP-100C-0017 from SPI Lasers UK Ltd) operating in $TEM_{00}$ mode and emitting at 1090 nm. The lasers are focused onto the sample from each side of the DAC using two 80 mm focal length achromatic lenses. Two Ag-coated carbon mirrors reflect the laser beams so that they are parallel with the x-ray beam and coincident at either side of the sample. Light emitted from the heated spot is reflected by the carbon mirrors and focused onto a pair of Acton 150i spectrometers with Hammamatsu CCD detectors (128 x 1024 pixels). Spectra collected during heating by these detectors are used to determine the sample temperatures

spectroradiometrically following the techniques discussed in Walter and Koga (2004). Optical aberrations induced by the refractive lens system are effectively minimized by selecting only paraxial radiation with a pair of adjustable iris diaphragm apertures ('f stops'). Calibration of the detector is made with a NIST-calibrated lamp of known spectral radiance, and temperatures calculated using an optimized wavelength range (typically 600 – 800 nm). Normalized spectra are fitted to the Wien equation, and the precision on fits are typically of the order 5 – 10 K, which is consistent with a minimum of chromatic aberration (Walter and Koga, 2004).

2.2 Experimental strategy

Figure 2 illustrates the basis for the experimental strategy. Spatially resolved pairs of ingredients are placed within the hole of a pre-indented gasket between the culets of the diamonds in a DAC. The contact edge between the reactants becomes the locus for step-wise laser heating from both sides to induce a chemical reaction, such as first melting. The eutectic melt of composition between the reactants forms a puddle at the heated interface by diffusive interchange between the reactants and the growing puddle. Chemical gradients within the liquids are expected to be small for experiments lasting seconds to minutes in duration because liquid metal diffusivities of order $10^{-4}$ $cm^2$/sec ensure exchange times across 20 micron spots of the order of a small fraction of a second. [For this reason, one may anticipate that quenching may not preserve an accurate record of the liquid state phase chemistry.] The growing puddle remains saturated in the reactants with which it is in contact. Increase of laser power, once first melting is reached, may not increase temperature, but instead may induce further melting as heat is consumed in the invariant reaction. This temperature plateau behavior confirms first

melting. If first melting temperature at pressure is already known from previous studies, the observation of this behavior provides a cross-check on experimental performance. Because the laser heating can be done at the same time that X-ray illumination occurs, the observations of a reaction product and its composition, or the absence of a product, can be done at experimental P and T. Although this technique saves the time and effort of subsequent examinations and analyses, the principal advantage is that the *in situ* observations have no quenching artifacts to unravel. This deliverance from the mists of quenching is uniquely important for experiments performed on charges whose size is a fraction of the characteristic diffusion length during quenching times and whose materials are highly reactive metal alloys where glasses are a headline novelty anyway. The ability to evaluate the experiment *in situ,* and then reexamine it after quench, inform the evaluation of whether DAC cell melting experiments in metal alloy systems are quenchable or not. We shall see that the answer to this question of quenchability is 'decidedly not' in a significant number of the systems we examined.

To the extent that the paired ingredients have an X-ray absorption contrast between them, the product liquid will be intermediate in its mass absorption coefficient – and hence X-ray absorption darkness – compared to the reactants. As reactants remain present outside the laser-heated spot, absorption standards for determining the eutectic liquid composition are present in each experiment. [We neglect for this analysis the density differences between the heated and unheated portions of the experiments because the total absorptive material in the beam path does not change appreciably if experimental geometry is maintained.] In as much as the seam between reactants in our hole-in-donut geometry for the disc-like composite of reactants has a circumference

(~120 microns) several times larger than the laser spot size (~20microns), it becomes possible to do more than one experiment per loading, for instance at more than one pressure.

The success of the technique for determining reaction product liquid composition depends strongly upon the ability to maintain uniform thickness (except for minor modulations due to thermal expansion under laser heating) throughout our composite hole-in-donut disc reaction couple. This requirement is especially challenging during the extensive compression to experimental pressures approaching half a megabar. Any deviation in the amount of material in the beam path changes the relative absorption experienced by various X-ray transit paths. The crux of our experimental strategy is to change the balance of heavy and light absorbers in the path by lateral diffusive transfer, without also adding a topographic modulation by lateral mechanical transfer under uniaxial compression. The complication of sample topography induced by mechanical flow provides an operational limit to the interpretation of X-ray absorption changes produced by chemical reaction. The uniformity of the absorption images of the paired reactants before and after first melting provides a check on whether this potential complication has compromised the result.

The maintenance of constant-thickness geometry would be substantially easier if the reactants had their thickness imposed by direct contact with the diamond culets themselves. Such a potential mechanical simplification however leads to experiment-ending complications such as the inability to heat the target because the diamonds too readily remove the laser-supplied heat. Should excess laser energy actually succeed in causing Fe melting, reactions with the diamonds chemically compromise the product and

mechanically compromise the diamonds with catastrophic result. For these reasons we employ a refractory insulating layer that is as chemically inert as possible between the composite disc and the diamond culets. For those experiments in which Fe-based melts are produced, $Al_2O_3$ was our preferred material. Different binary systems might employ different materials.

$Al_2O_3$ insulation makes the experiments possible at one level; at another level it significantly complicates the topography/chemistry convolution because the sample and the $Al_2O_3$ have rheological mismatches for accommodating any initial gaps and void spaces in the experimental fabrication. In our initial setup we drilled a large hole (~ 200 μm) in a pre-indented gasket of Re and filled the hole with iron powder. The powder was re-compressed to ~ 5 to 10 GPa forming a new, composite gasket. A second ~ 50 μm hole was the drilled in the iron and filled with FeS and re-compressed. Finally, a dollop of sub-micron $Al_2O_3$ powder was placed above and below the sample so that loose powder covered the sample, the gasket, and filled any void spaces. In this geometry, compression quickly developed a waffled texture with ring-dikes of Fe forming through the $Al_2O_3$. This strategy did not produce interpretable results beyond 10 GPa. To mitigate against these mechanical instabilities we developed a new strategy of producing a set of close-fitting discs of sample reactants and dense $Al_2O_3$.

The sample disc is fabricated as follows: (1) Pure hardened iron foil is indented in a DAC to ~15 GPa, which yields a metal thickness of ~ 20-30 μm. (2) The indented metal is then drilled with a 50 μm hole, which is loaded with powdered FeX (= FeS, $Fe_3C$, FeSi, FeO(OH), or FeO) and compressed until the material is sufficiently compacted to remain in place. (3) An ~100 μm diameter disc consisting of the central

plug of FeX and an annulus of iron (a sample 'donut') is then cut out using an automated UV laser cutting system. The sample disc is then polished using 1 μm diamond impregnated mylar to a thickness of ~ 15-20 μm, and cleaned under acetone and stored in an oven at 125°C until loading.

Prefabricated $Al_2O_3$ discs to sandwich the sample donut in the gasket hole are made as follows. $Al_2O_3$ powder (0.3 micron) is pressed by hand between glass slides to a thickness of ~30 microns. A stock solution of 50% aluminum sec-tributoxide (ASB), 30% isopropanol, and 20% acetylacetone is prepared. The ASB stock solution is diluted before use by another factor ~4 with isopropanol. The compressed powder is saturated with the diluted ASB solution and gently heated to evolve moisture. After drying, the powder has enough coherence to be delaminated from the glass slide with a razor blade, like shingles off a roof. The shingles are fired from 500-900 ºC overnight. From the debris, selected delaminated shingles are cut into discs with a diameter (~110 μm) equal to that of the sample donut and gasket hole (i.e. all are laser cut using the same pattern). A hard firing overnight at 900 ºC in a quartz tube gives the resulting muffins sufficient coherence to be stored in glass bottles until needed. The close-fitting character of the muffins and composite sample donut to the gasket hole with minimal slop of $Al_2O_3$ between the diamonds and gaskets leads to successful uniform compression up to ~40 GPa, after which topographic complexity again begins to make radiographic images difficult to interpret. Figure 3 illustrates this configuration for an Fe donut stuffed with FeO. Evolution to still more-closely-fitting designs may be able to extend the technique to the full range of DAC pressures.

Pressures were increased by tightening the screws of a symmetrical DAC. Pressure was monitored by ruby fluorescence before and after heating. Pressure can drop significantly during heating and pressure gradients across the gasket holes monitored by several ruby chips are less than ~1 GPa. In the experimental sequences we report, the initial pressure and the final pressure after heating are shown in the figures. We report the relaxed pressure after the experimental heating when giving the composition of the liquid produced. We neglect any thermal pressure that may have been present *in situ*. Unfortunately in our current 12.2.2 configuration it is not possible to perform imaging and diffraction in the same experiment. However such a refinement is not impossible and future experimental programs may be able to use diffraction from an added internal standard or the unreacted Fe to assess the *in situ* pressure.

Starting materials for the experiments include 250 micron thick hardened Fe sheet supplied by Goodfellow Metals from which sample discs are fabricated. FeS filling was synthetic troilite prepared by reacting reagent Fe and S powders in a silica tube during a slow ramp to 1000 ºC. FeO filling was prepared from Puratronic Fe bar in a $H_2$-$CO_2$ gas stream one log unit in $pO_2$ above the Fe-wustite buffer at 1200 ºC overnight. $Fe_3C$ was prepared at 1200 ºC and 2 GPa in a piston-cylinder apparatus by Dr. Rajdeep Dasgupta from a mixture of Fe and diamond powder. FeO(OH) was supplied by Prof. A. Navrotsky.

3.1 Results: Fe-FeS

Figure 4 shows a pair of X-radiographic images and corresponding absorption profiles across the lozenge of first melt grown at the Fe-FeS interface of experiment FS-

21, performed using our initial loading strategy. These images are representative of the quality of image produced in this study. There are clear departures from the idealized image of Figure 2. The boundaries between phases are not vertical in the absorption profiles because there is undoubtedly slurring of the boundary mechanically, and possibly chemically. The absorption density of the image across the Fe and the FeS is not perfectly uniform. A waffled texture is developing which becomes rapidly worse with increasing pressure in these early "dollop of alumina powder" insulator strategy experiments. And still at 4 GPa the image is easily interpretable. The appearance of the melt lozenge in the image and the ledged absorption profile were obvious and dramatic during a single step in the heating cycle. The absorption intensity position of the melt ledge between the ledges for Fe and FeS gives a composition for the liquid in proportion to the saturating end members of 27±1.4 wt. % S, which is in satisfactory agreement with both Ryzhenko and Kennedy (1973) and Usselman (1975) because the 4 GPa of this experiment after heating is below the pressures where these earlier determinations of the eutectic composition diverge from one another.

Figure 5 shows some images in a sequence from experiment FS-55 at significantly higher pressure using the 'muffin sandwich' approach to insulation: A. cold 17 GPa before heating, B. during first melting, and C. upon quenching to a relaxed pressure of 16 GPa. This experiment, showing development and preservation of the melt blob at the interface of Fe and FeS, is seen to be virtually free of the waffle texture that complicates Figure 4. There is a slight suggestion at this and higher pressures that the quenched absorption ledge shifts to marginally less S-rich compositions shown in Figure 6, although this quench-shift effect is within the errors quoted for each measurement,

giving only a small suggestion that liquid quenchability is not perfect. Even so, neither composition is noticeably discrepant compared to the literature values of the Fe-FeS eutectic composition as a function of pressure recorded in Figure 6. This concordance applies to all 4 of our experiments to 20 GPa, giving some reinforcement to the ideas that the radiographic technique works and that the system Fe-FeS is quenchable at some level, however imperfectly. This pair of conclusions is made stronger by the fact that the eutectic composition shows variation as a function of pressure and that there is reasonable agreement between investigators using a range of techniques.

Figure 7 shows the sequence of images and profiles for experiment FS-52, further raising the importance of making *in situ* observations. This experiment initially at 45 GPa coupled poorly to the laser at first and then melted suddenly with a burst at a temperature measured spectroradiometrically to be 2100 K, more than 100 K above the expected eutectic in the neighborhood of 40 GPa. The growth of the melt bubble was sudden but showed a reasonable ledge structure in the absorption profile giving 18±0.5 wt. % S in the liquid, a composition much too S-rich for the eutectic from the literature results of Chudinovskikh and Boehler (2007), or from our projections from 20 GPa. We believe we have exceeded the eutectic temperature and are on the S-rich branch of the liquidus. On further heating, a curious brighter bump develops near the Fe that shows up as a dip and a bump in the absorption profile where previously there was a liquid ledge before quenching. This dip and bump structure is preserved on quenching. It appears as if there was transfer of material to place more S-rich material than the liquid against the Fe, perhaps by precipitation of crystalline material. Crystalline $Fe_3S_2$ (27.7 wt.% s) is more Fe-rich than troilite and more S-rich than our liquid, and has been reported before at

high pressure by Fei et al. (1997, 2000) at rather lower temperature. This compound and $Fe_3S$ (16 wt. % S) complicate the melting relations so that a stable Fe-FeS eutectic may no longer exist. Moreover $Fe_2S$ with 22.3 wt. % S (also reported by Fei et al., 2000) is closer in composition to the bright bump, but is still an imperfect match, so that the constitution of this bright bump is unclear. Because the liquid at 18 wt. % S is compositionally exterior to both $Fe_2S$ and FeS, it is tempting, but currently unwarranted, to offer this image as an example of the peritectic relation of liquid to the $Fe_2S$ + FeS assemblage suggested by Fei at al. (2000) at much lower pressure and temperature. The complexity of this behavior is difficult to interpret at present and emphasizes the importance of making *in situ* measurements as structures develop in this sort of system at these tiny scales to help rationalize the complexities seen after quenching.

This indication is strongly reinforced by a sequence of absorption profiles in Figure 8 from experiment FC-45 in which the filling in the Fe donut was $Fe_3C$ instead of FeS. A well-developed ledge grew on first melting at 2160 K giving composition of 2.2±0.5 wt. % C in the liquid at 27 GPa. Upon quenching, the ledge disappears, or more exactly it decays into a vague sloping profile of lesser slope than the sloping boundary between Fe and $Fe_3C$. This is a clear indication of quenching difficulties that were observed in several other Fe-$Fe_3C$ experiments. Those experiments and additional ones in Fe-FeSi had frequent failures to quench that are reported in a companion paper.

## 3.2 Results: Fe-O-H

The question of the solubility of oxygen in liquid metal at high pressure has driven our investigation from the start. Our study of Fe-FeS was motivated by our initial

failures to discover anything like the ledge profile and blob image results we anticipated for Fe-FeO from the strategy proposed by Walker (2005) and outlined in Figure 2 and seen in Fe-FeS and related systems. We sought to see if we could reproduce known answers with our technique, and we feel that we have been able to do so in Fe-FeS, at the same time we rediscover the importance of avoiding quenching techniques where possible in metal-based systems. The importance of *in situ* measurements in systems like this has previously been emphasized by Tsuno et al. (2007). The reason we have targeted Fe-FeO especially is that the issue of oxygen solubility in liquid metal at high pressure is contentious and consequential.

It has long been known (Darken and Gurry, 1946) that the first melting of Fe with oxygen present shows little oxygen solubility in the liquid metal (~0.2 wt %). Ringwood (1984) was an early champion of the idea that oxygen solubility on first melting would increase dramatically with high pressure and, therefore, oxygen might be a viable candidate for the light element alloyed in the liquid metal outer core. His supporting arguments were substantially based on the volume of oxygen in solution in liquid metal. The experimental work of Ohtani et al. (1984) at quite modest pressure was interpreted to support this view of increasing oxygen solubility with pressure. The idea gained traction from the DAC work of Knittle and Jeanloz (1991) and Goarant et al. (1994). Both groups claimed significant reactivity between liquid metal and Fe-bearing silicates and oxides at pressures over 30 GPa which they interpreted to be the result of FeO in solution in the silicates and oxides becoming soluble in liquid metal and reacting accordingly. This work was controversial because the extent of a reaction is difficult to estimate in quenched experiments (Boehler, 2000). Furthermore, studies of the solubilities of oxides

in liquid Fe-based metals at multi-anvil pressures by O'Neill et al. (1998) and Rubie et al. (2004) have not supported the view that oxygen becomes more soluble with pressure. These authors interpreted the reaction volumes for putting oxygen into solution to be unfavorable and therefore oxygen should become less soluble with increasing pressure. Walker et al. (2002) reviewed the oxygen reaction volume problem in the light of new measurements of the partial molar volumes of oxygen in a variety of exotic compounds, with the conclusion that increasing oxygen solubility was much more probable than supposed by O'Neill and coworkers. Walker (2005) put these considerations into a context where, even if oxygen solubility did temporarily decrease for the first couple 10s of GPa in pressure, it would almost surely increase by half a megabar.

This prediction raises the central question for evaluation with the X-ray absorption imaging technique proposed by Walker (2005) and reported here. ***Does oxygen solubility jump to 2% or to 20%, or to some other level, when pressure approaches a megabar?*** This is a question to which the volume arguments can only supply a qualitative answer, so that new measurements of solubility are required. Some of them have begun to appear from quenching studies in DAC (Takafuji et al., 2005; Asahara et al., 2007) and from the *in situ* study of Seagle et al. (2008) with the result that solubilities approaching a megabar are modest, and limited to ~12%. Our attempts to use X-ray absorption imaging to measure the melting reaction between Fe and FeO fit into this context.

Experiment FO-50 was heated sequentially to 2700-3000 K at 35 GPa without a ledge and blob result or any other sign of reactivity. This temperature and pressure achieve the threshold of reactivity outlined by Knittle and Jeanloz (1989) between Fe and

372 silicates. Furthermore 2700 K exceeds the Fe-FeO eutectic temperatures at this pressure
373 of both Boehler (1992) and Seagle et al. (2008) by at least 400 K. Indeed we observe the
374 power-temperature hesitation associated with initiation of melting in the recommended
375 region. Figure 9 shows X-radiographic images from experiment FO-58 for a series of
376 compressions out to 41 GPa, demonstrating that the new loading techniques work well
377 enough to preserve good Fe-FeO phase interfaces for heating. The absorption profiles
378 during progressive heating to 2300-2500 K at 40 GPa [up to or slightly in excess of the
379 Fe-FeO eutectic of Boehler (1992) and Seagle et al. (2008)] are again singularly
380 uninteresting except to show that the boundary is well preserved. No ledges develop and
381 no interfacial blobs are formed. Our failure to observe reactivity in Fe-FeO is not a
382 consequence of obtaining uninterpretably complex images. Profiles from experiment
383 FO-47, not shown, have a similar lack of reactivity to temperatures of 2500-2860 K at 43
384 GPa. This temperature and pressure are marginally within the area of expected reactivity
385 between Fe and silicates outlined by Knittle and Jeanloz (1989) and substantially exceed
386 the eutectic temperatures of Seagle et al. (2008). And yet, in short, nothing observable
387 happened, a result entirely consistent with our previous lack of results in Fe-FeO before
388 we turned to Fe-FeS for comfort and encouragement. Our detectability limit for these
389 images is about 1-2% oxygen, suggesting that any melt generated has less than this
390 amount of oxygen. These results are unsupportive of the view that oxygen becomes
391 highly soluble in liquid Fe by 40 GPa, and is in contrast to the ~ 6 wt% oxygen predicted
392 by the results of Seagle et al.(2008) at this pressure. It is possible that Seagle's technique
393 can record false positives because phase diffraction disappearance may be a consequence
394 of other processes than dissolution. It is also possible that our technique can give false

395 negatives for FeO for unknown reasons even when it does show positives for FeS, $Fe_3C$,
396 FeSi, and FeO(OH) even at fairly low levels of solubility. We are considerably more
397 comfortable offering our non-results from Fe-FeO in the context of having shown that the
398 technique does not always give false negatives.

399 If oxygen were more soluble, then a number of drivers for core to mantle
400 chemical transfer might operate as discussed by Walker (2005). Alexandra Navrotsky
401 (public comment at the 2006 COMPRES meeting) suggested that the formation and
402 solution of Fe hydrides could cause some of the same transfer mechanisms to operate
403 without oxygen. To screen this proposition she supplied us with an Fe hydroxide
404 powder. Figure 10 shows the absorption profiles across experiment FOH-57 that had its
405 donut hole stuffed with the hydroxide. Laser heating of the interface produced
406 recognizable reactivity of the blob and ledge type now so familiar to us from experiments
407 on FeS, $Fe_3C$, and FeSi fillings. Unfortunately the possibility that the (OH) groups may
408 disproportionate in the reaction and render the system ternary means that we can do little
409 to evaluate the compositional details of this reaction. Thus Prof. Navrotsky's excellent
410 suggestion must remain only a possibility that we cannot further evaluate with this
411 technique.

412 However, as outlined by Walker (2005), the chemical topology of the reaction can
413 be determined from the image. Odd reactions (peritectic type in binary or chemically
414 more complex systems) can be recognized from the X-ray image if one of the reactants
415 grows with the product at the expense of the other reactant(s). This finding can be
416 confirmed from the absorption profile if the product is not intermediate between the two
417 reactants in composition. Should a $4^{th}$ phase appear, or be present initially in a ternary

system, the reactant X-ray absorptivity is less useful an index. However the observation of which phases are consumed and which phases grow remains a powerful constraint on the chemographic reaction type. In the case of figure 10, the reaction is clearly of the even type because both reactants are being eroded by the growth of the reaction product. That there is a reaction product at all reinforces the bleakness of the non-findings in the Fe-FeO system.

## 4. Summary

Progress has been made in implementing X-radiography as an aid to making *in situ* binary chemical observations of experiments whose dimensions are smaller than the diffusion quenching length, for instance of metallic liquids in DAC. The technique appears to confirm previous work in the system Fe-FeS on the composition of the eutectic with pressure. The technique fails to detect much solubility of oxygen in molten Fe at pressures to 43 GPa.

## Acknowledgements

We would like to thank the staff of the ALS for help and encouragement in developing the X-ray imaging system. In particular we would like to acknowledge the help of Alastair MacDowell, Howard Padmore, Martin Kunz and Jason Knight. The Advanced Light Source is supported by the Director, Office of Science, Office of Basic Energy Sciences, of the U.S. Department of Energy under Contract No. DE-AC02-05CH11231. The activities on beam line 12.2.2 are supported by COMPRES. We thank Prof. Alexandra Navrotsky for her suggestion of

exploring the hydrides and her supplying of the FeO(OH) powder. We thank Dr. Rajdeep Dasgupta for the $Fe_3C$ starting material, and L. Armstrong for assistance at the beamline. DW acknowledges support from NSF/EAR and COMPRES. MJW acknowledges support from NERC grant NE/C511548/1. LDEO Contribution #xxxx.

References:

Asahara Y, Frost DJ, Rubie DC, 2007. Partitioning of FeO betweenmagnesiowustite and liquid ironat high pressures and temperatures: implications for the Earth's outer core. Earth Planet. Sci. Lett. 257, 235-249.

Birch F, 1952. Elasticity and constitution of the Earth's interior. J. Geophys. Res., 57, 227-286.

Boehler, R., 1992. Melting of the Fe–FeO and the Fe–FeS systems at high pressure — constraints on core temperatures. Earth Planet. Sci. Lett. 111, 217–227.

Boehler R, 2000. High pressure experiments and the phase diagram of lower mantle and core materials. Rev. Geophys., 38, 221-245

Brett, R. and Bell, P.M., 1969. Melting relations in the Fe-rich portion of the system Fe-FeS at 30 kb pressure. *Earth and Planet. Sci. Lett. 6*, 479-482.

Caldwell W.A., M. Kunz, R.S. Celestre, E.E. Domning, M.J. Walter, D. Walker, J. Glossinger, A.A. MacDowell, H.A. Padmore, R. Jeanloz and S.M. Clark, 2007. Laser Heated Diamond Anvil Cellpage at the Advanced Light Source Beamline 12.2.2. Nuclear Instrumentation and Methods in Physics Research, Section A 582, 221-225.

Chudinovskikh L and Boehler R, 2007. Eutectic melting in the system Fe-S to 44 GPa. Earth and Planet. Sci. Lett. 257, 197-203.

Darken LS and Gurry RW, 1946. The system Iron-Oxygen. II. Equilibrium and thermodynamicsof liquid oxide and other phases. J. Amer. Chem. Soc. 68, 799-816.

Fei YW, Bertka CM, and Finger LW, 1997. High pressure iron sulfur compound $Fe_3S_2$, and melting relations in the Fe-FeS system, Science 275, 1621-1623.

Fei YW, Li J, Bertka CM, and Prewitt CT, 2000. Structure type and bulk modulus of $Fe_3S$, a new iron-sulfur compound, American Min. 85, 1830-1833.

Goarant F., Guyot F., Peyronneau J., and Poirier J-P, 1992. High-pressure and high-temperature reactions between silicates and liquid iron alloys, in the diamond anvil cell, studied by analytical electron microscopy. J. Geophys. Res. 97, 4477-4487.

Gurvich A.M., V.B. Gutan, B.N. Meleshkin, V.V. Mikhailin, A.A. Mikhalev and M.I. Tombak, 1977. On the nature of optically active centers in self activated luminophors of the $CaWO_4$ type, J. of Luminescence 15, 187-199.

Knittle E. and Jeanloz R., 1998. Simulating the core-mantle boundary: an experimental study of high-pressure reactions between silicates and molten iron. Geophys. Res. Lett. 16(7), 609-612.

Knittle E. and Jeanloz R., 1991. Earth's core-mantle boundary: results of experiments at high pressures and temperatures. Science 251**,** 1438-1443

Kunz M., A.A. MacDowell, W.A. Caldwell, D. Cambie, R.S. Celestre, E.E. Domning, R.M. Duarte, A.E. Gleason, J.M. Glossinger, N. Kelez, D.W. Plate, T. Yu, J.M. Zaug, H.A. Padmore, R. Jeanloz, A.P. Alivisatos, and S.M. Clark., 2005. A beamline for high pressure studies at the Advanced Light Source with a superconducting bending magnet as the source. J. Synch. Rad. 12(5), 650-658.

Li J, Y Fei, HK Mao, K Hirose, and S Shieh, 2001. Earth Planet. Sci. Lett. 193, 509-514.

Morard G, Sanloup C, Fiquet G, Mezouar M, Rey N, Poloni R, and Beck P (2007) Earth Planet. Sci. Lett. 263, 128-139.

Ohtani E., Ringwood A.E., and Hibberson W., 1984. Composition of the core, II. Effect of high pressure on solubility of FeO in molten iron. Earth Planet. Sci. Lett. 71, 94-103.

O'Neill H.St.C., Canil D., and Rubie D.C., 1998. Oxide-metal equilibria to 2500$^{o}$C and 25 GPa: implications for core formation and the light component in the Earth's core. J. Geophys. Res. 103, 12239-12260.

Poirier J-P, 1994. Light elements in the Earth's outer core: a critical review. Phys. Earth Planet. Int. 85, 319-337.

Rhyzenko B and GC Kennedy, 1973. Effect of pressure on the eutectic insystem Fe-FeS. Amer. J. Science. 273, 803-810.

Ringwood AE, 1984. The Earth's core: its composition, formation, and bearing upon the origin of the Earth. Proc. R. Soc. London, Ser. A, 395, 1-46.

Rubie D.C., Gessmann C.K., and Frost D.J., 2004. Partitioning of oxygen during core formation on the Earth and Mars. Nature 429, 58-61

Seagle CT, Heinz DL, Campbell AJ, Prakapenka VB, Wanless ST, 2008. Melting and thermal expansion in the Fe-FeO system at high pressure. Earth Planet. Sci. Lett. 265, 655-665.

Stampanoni M., G. Borchert, P. Wyss, R. Abela, B. Patterson, S. Hunt, D. Vermeulen and P. Ruegsegger, 2002. High resolution x-ray detector for synchrotron based microtomography, Nuclear Instruments and Methods A491, 291-301.

Takafuji N, Hirose K, Mitome M, Bando Y, 2005, Solubilities of O and Si in equilibrium with $(Mg,Fe)SiO_3$ perovskite and the light elements in the core. Geophys. Res. Lett. 32, L06313, doi:10.1029/2005GL022773.

Tsuno K, Terasaki H, Ohtani E, Suzuki A, Asahara Y, Nishida K, Sakamaki T, Funakoshi K, Kikegawa T, 2007. In situ observation and determination of liquid immiscibility in the Fe-O-S melt at 3 GPa using a synchrotron X-ray radiographic technique. Geophys. Res. Lett., 34, L17303, doi:10.1029/2007/GL030750.

Usselman, T.M., 1975. Experimental approach to the state of the core: Part I. the liquidus relations of the Fe-rich portion of the Fe-Ni-S system from 30 to 100 kb. Am. J. Sci. 275, 278-290

Walker D., S.M. Clark, L.M.D. Cranswick, M.C. Johnson, and R.L. Jones., 2002. $O_2$ volumes at high pressure from $KClO_4$: D" as a siderophile element pump instead of a lid on the core. Geochemistry Geophysics Geosystems, 3, *#11*, 26 pages, 23 November 2002, paper GC000225.

Walker D, 2005. Core-mantle chemical issues. *Can. Mineralogist*, **43**, 1553-1564.

Walter MJ and Koga KT, 2004. The effects of chromatic dipersion on temperature measurement in the laser-heated diamond anvil cell. Phys. Earth and Planet Int. 143-144, 541-558.

**Table 1 Experimental results**

| Experiment | exposure | temperature | pressure | first liquid composition | |
|---|---|---|---|---|---|
| **Fe-FeS** | # | T ± 10K | P Gpa † | Wt. % S | ± |
| FS-21 | 26 | * | 4 | 27 | 1.4 |
| FS-56 | 30 | * | 7 | 26.4 | 1 |
| FS-55 | 2 | * | 16 | 19.7 | 1.8 |
| FS-55 | 11 | 1730 | 20 | 16.9 | 1.3 |
| FS-52 | 3 | 2100 | 34 | 18.2 | 0.5 |
| **Fe-FeO(OH)** | | | | Wt. % O(OH) | ± |
| FOH-57 | 37 | 2680 | 12 | 14.5 | 1.1 |
| **Fe-FeO** | | | | Wt.% Oxygen | |
| FO-50 | 10 | 2590 | 35 | undetected | |
| FO-58 | 10 | 2530 | 40 | undetected | |
| FO-47 | 24 | 2570 | 43 | undetected | |
| FO-47 | 29 | 2500 | 43 | undetected | |

* T too low to determine reliably
† pressure after heating

Figure Captions

Figure 1 Photograph of components of ALS Beam line 12.2.2 around the diamond anvil cell (DAC) holding imaging experiments.

Figure 2 A. Schematic illustration of the configuration within a diamond anvil cell. The gasket surrounding the donut composite and alumina insulating discs is cut away so that the internal loading can be seen more clearly. B. Anticipated X-radiographic image of A with intensity profile along the line of section given. Phase composition for the first melting eutectic liquid determined as proportion of the intensity between compositions of the saturating phases Fe and FeX where FeX is variously FeS, FeSi, $Fe_3C$, FeO(OH), or FeO. The boundaries between phases are shown as sharp and the phase compositions by absorption intensity as uniform. Neither of these idealized situations is exactly realized

in experiments. Deformation during compression introduces some topographic complexity to the sample and some obliqueness to the phase boundaries.

Figure 3 Light photomicrograph in both transmitted and incident illumination of a stuffed donut sandwich experiment loaded within a DAC. Fe donut with FeO stuffing fits snuggly within the gasket hole and is covered with transparent $Al_2O_3$. Culet edge is 300 μm in diameter. Donut is ~110 μm in diameter.

Figure 4 X-radiographic images of experiment FS-21 and corresponding intensity profiles across the *in situ* experimental image of the second panel. Culet edge is 300 μm in diameter. Deviations from the ideality of Figure 1 include the waffled topographic texture of the Fe and the FeS, and the non-sharp boundaries between the liquid and its saturating phases, Fe and FeS. Even so the image is quite interpretable in terms of the liquid composition, and agrees quite well with the known literature value (see figure 6). This image is typical of what is interpretable. Some images are more nearly ideal as in Figures 2 or 4, but some are less so and are still interpretable. The value for the eutectic liquid's composition is 27±1.4 wt% S at 4 GPa.

Figure 5 X-radiographic images of experiment FS-55 ending when relaxed after quenching at 16 GPa. Fe donut is ~110 μm in diameter. The use of prefabricated alumina 'muffin' insulators to sandwich the donut composite leads to considerably less waffling of the sample under high compression.

Figure 6 Summary of literature information on the composition of the Fe-FeS eutectic as a function of pressure. Eutectic results from the current study given in red. Experiment FS-52 which was overheated beyond the eutectic and showed complex quenching behavior in Figure 7, is shown in grey at 34 GPa. All the eutectic results seem to be in reasonable agreement and are a strong function of pressure, suggesting the viability of the technique and that under some circumstances Fe-FeS experimental liquids are nearly quenchable.

Figure 7 X-radiographic images and absorption profiles of experiment FS-52 which overshot the Fe-FeS eutectic temperature substantially. Fe donut is ~110 μm in diameter. Complex behavior is observed *in situ* to develop during the heating and is preserved in both the quench image and its absorption profile. This behavior would be difficult to interpret were it only observed in a quench image.

Figure 8 Absorption profiles of experiment FC-45 in which the donut filling was $Fe_3C$. Fe donut is ~110 μm in diameter. There is a clear degradation of the first melting ledge upon quench with the liquid compositional ledge slumping into a ragged slope over an average compositional range that is half the *in situ* value. This unquenchable behavior is frequently encountered in systems Fe-$Fe_3C$ and Fe-FeSi that we report on elsewhere and contrasts with the typical behavior in Fe-FeS which is semiquenchable.

Figure 9 X-radiographic images and absorption profiles in experiment FO-58 in which the donut filling was FeO. Fe donut is ~110 μm in diameter. The images show a sequence of progressing compressions to 41 GPa during which some topographic complexity is introduced to the image by deformation. The absorption profiles (all at 41 GPa) show no development of a ledge for the first melting even at 2530 K.

Figure 10 X-radiographic images and absorption profiles for experiment FOH-57 in which the donut filling was FeO(OH). Fe donut is ~110 μm in diameter. A reactive ledge develops on heating - unlike in Fe-FeO experiments. X-ray absorption imaging is not useful for the determination of the reacted liquid composition unless the (OH) enters the liquid without disproportionation, which is currently unknown. Departures from binary behavior cannot be detected with this method. However it is safe to say from the imaging that because both reactants are eroded and the compositional ledge is intermediate to the end members, the reaction is even, not odd, in the chemographic sense.

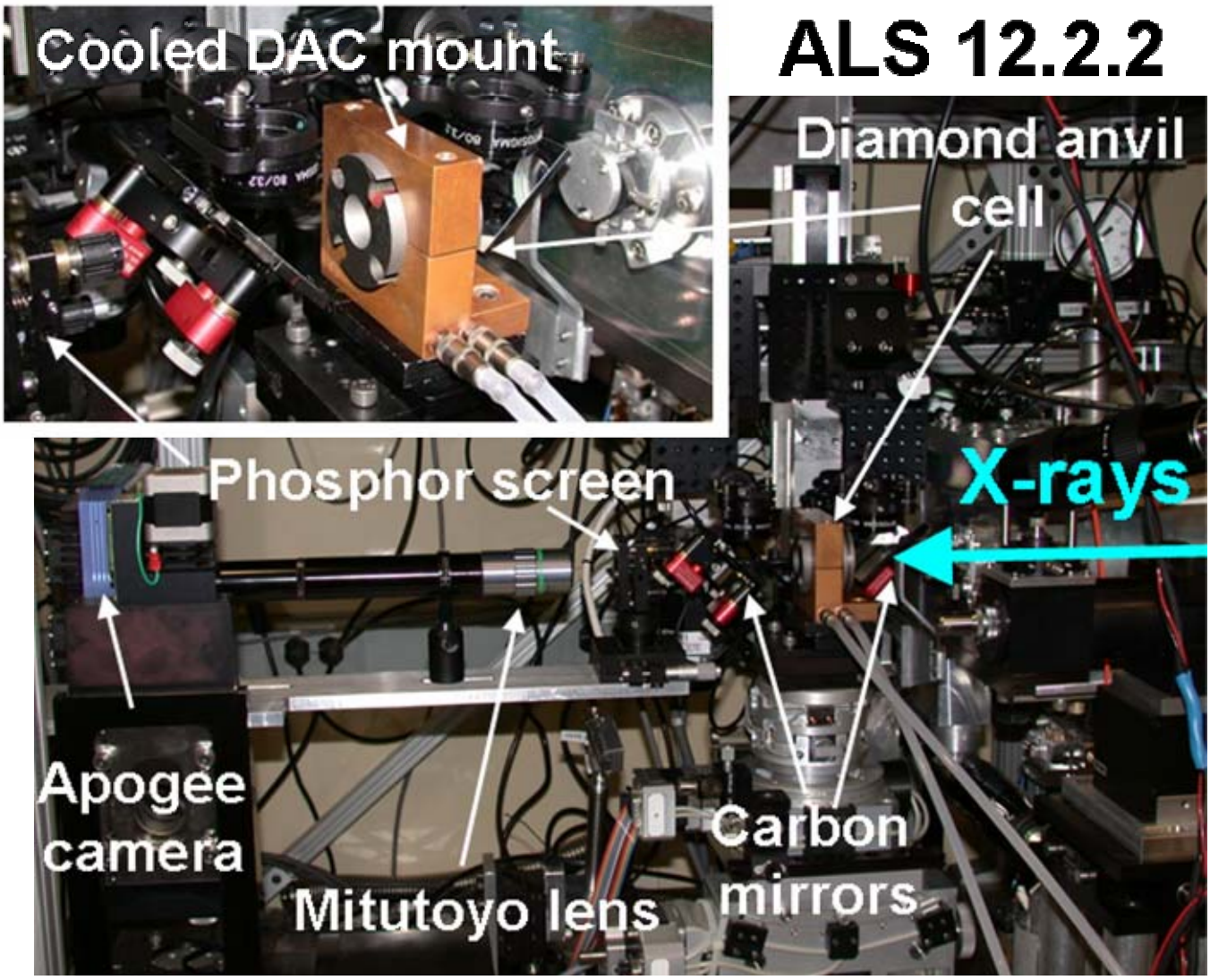


Figure 1 Photograph of components of ALS Beam line 12.2.2 around the diamond anvil cell (DAC) holding imaging experiments.

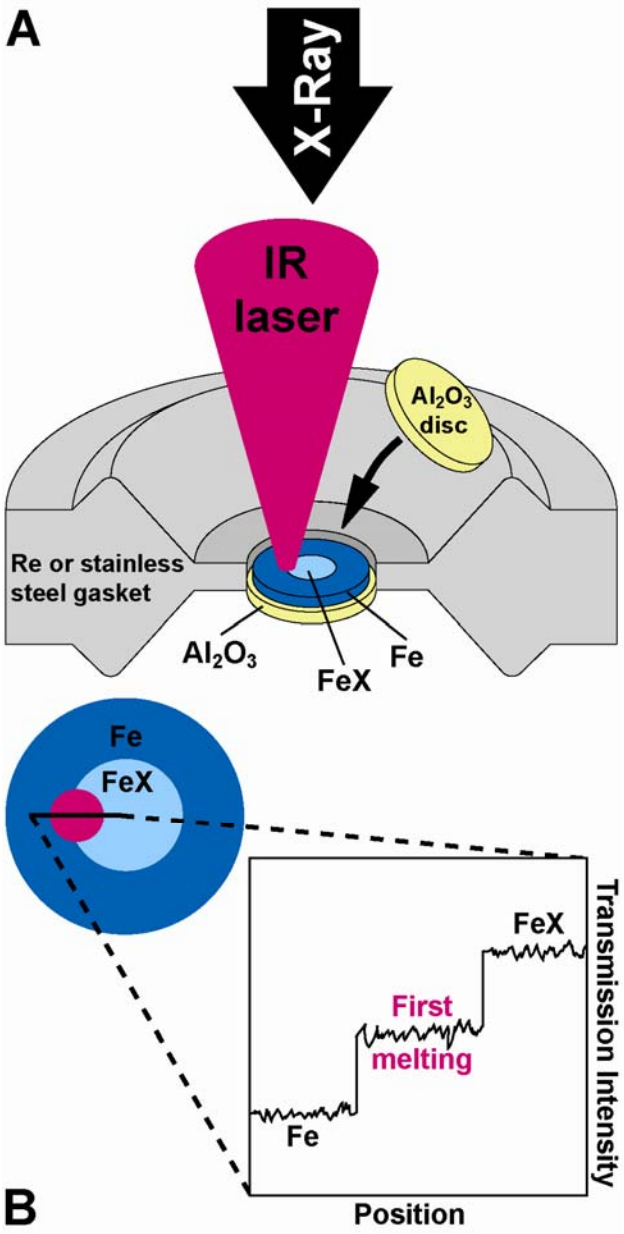


Figure 2 A. Schematic illustration of the configuration within a diamond anvil cell. The gasket surrounding the donut composite and alumina insulating discs is cut away so that the internal loading can be seen more clearly. B. Anticipated X-radiographic image of A with intensity profile along the line of section given. Phase composition for the first-melting eutectic liquid determined as proportion of the intensity between compositions of the saturating phases Fe and FeX where FeX is variously FeS, FeSi, $Fe_3C$, FeO(OH), or FeO. The boundaries between phases are shown as sharp and the phase compositions by absorption intensity as uniform. Neither of these idealized situations is exactly realized

in experiments. Deformation during compression introduces some topographic complexity to the sample and some obliqueness to the phase boundaries.

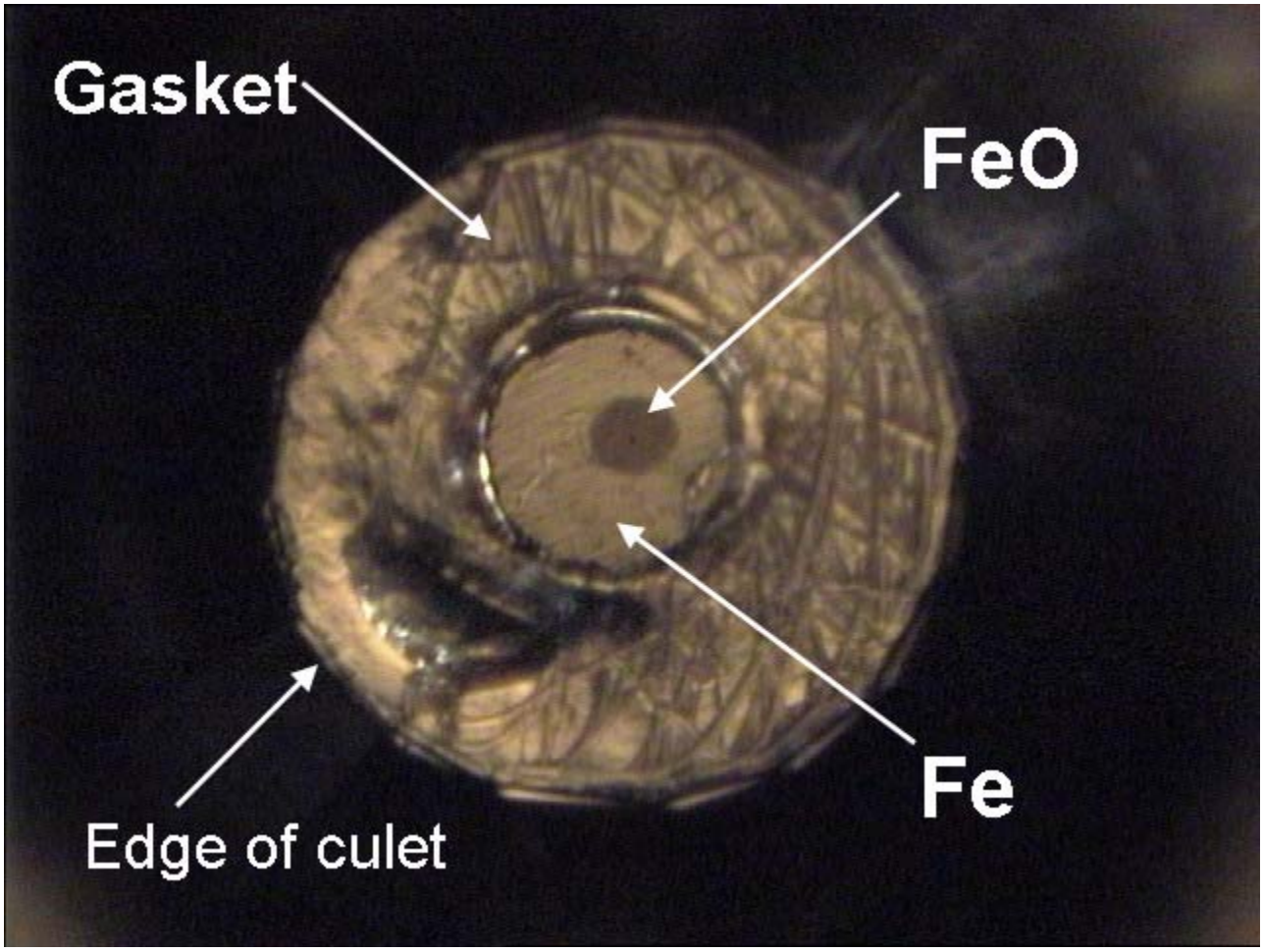


Figure 3 Light photomicrograph in both transmitted and incident illumination of a stuffed donut sandwich experiment loaded within a DAC. Fe donut with FeO stuffing fits snuggly within the gasket hole and is covered with transparent $Al_2O_3$. Culet edge is 300 μm in diameter. Fe donut is ~110 μm in diameter.

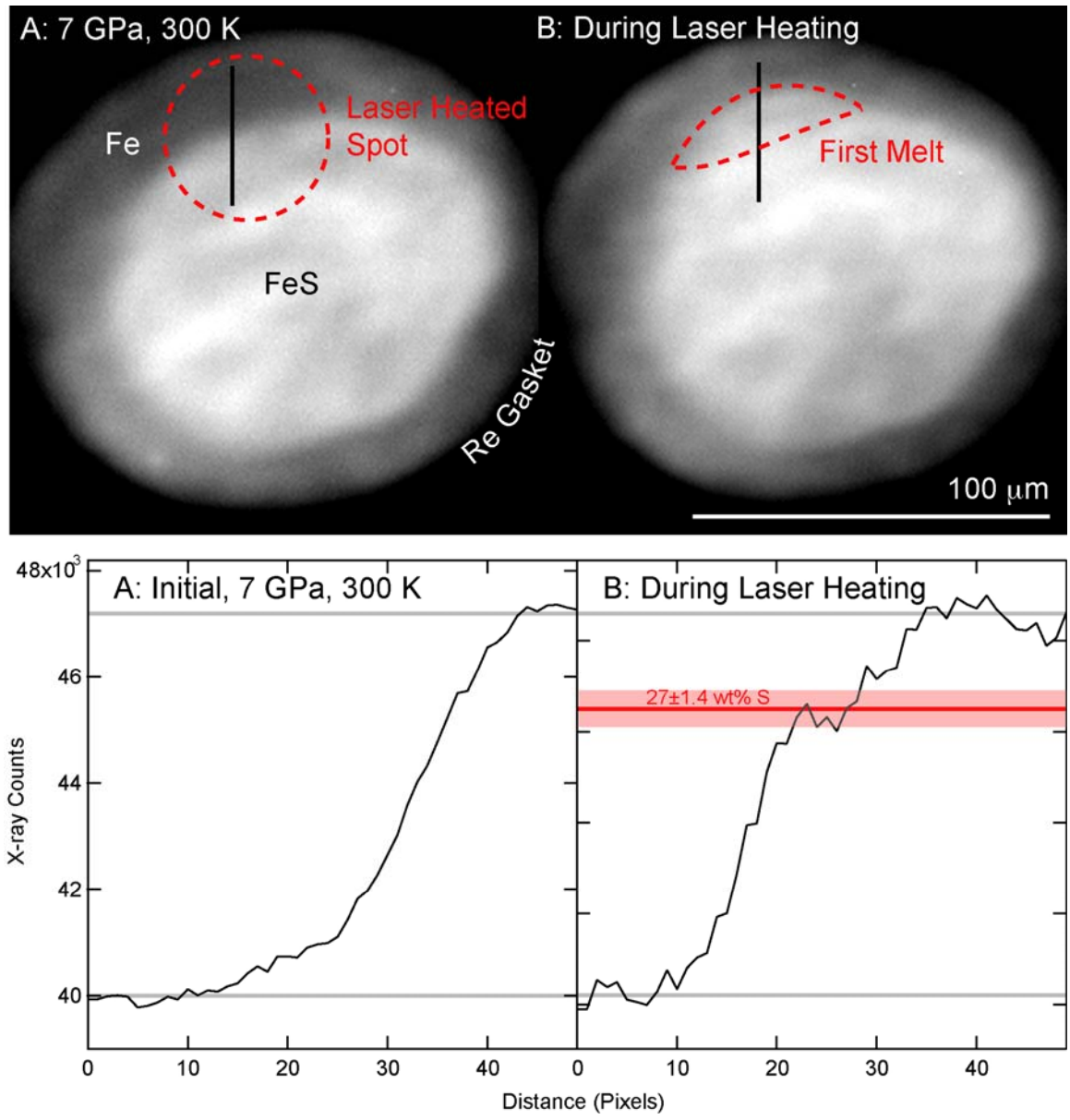


Figure 4 X-radiographic images of experiment FS-21 and corresponding intensity profiles across the *in situ* experimental image of the second panel. Deviations from the ideality of Figure 1 include the waffled topographic texture of the Fe and the FeS, and the non-sharp boundaries between the liquid and its saturating phases, Fe and FeS. Even so the image is quite interpretable in terms of the liquid composition, and agrees quite well with the known literature value (see figure 6). This image is typical of what is interpretable. Some images are more nearly ideal as in Figures 2 or 4, but some are less so and are still interpretable. The value for the eutectic liquid's composition is 27±1.4 wt% S at 4 GPa.

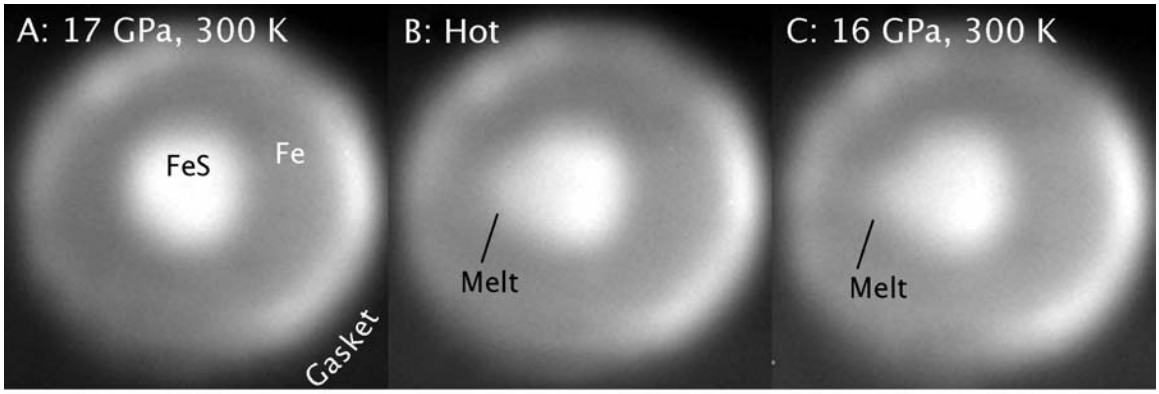


Figure 5 X-radiographic images of experiment FS-55 ending when relaxed after quenching at 16 GPa. Fe donut is ~110 μm in diameter. The use of prefabricated alumina 'muffin' insulators to sandwich the donut composite leads to considerably less waffling of the sample under high compression.

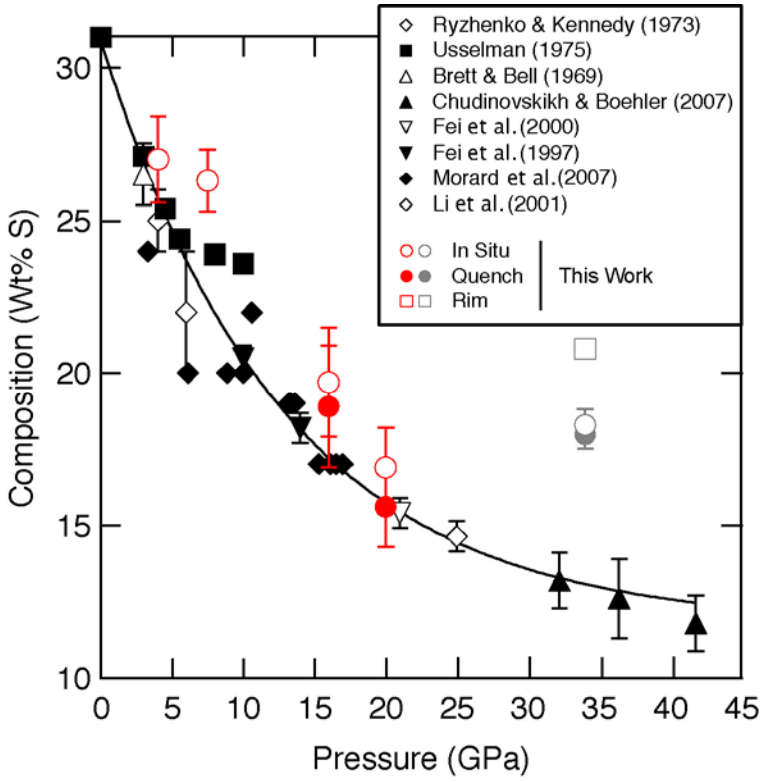


Figure 6 Summary of literature information on the composition of the Fe-FeS eutectic as a function of pressure. Eutectic results from the current study given in red. Experiment

FS-52 which was overheated beyond the eutectic and showed complex quenching behavior in Figure 7, is shown in grey at 34 GPa. All the eutectic results seem to be in reasonable agreement and are a strong function of pressure, suggesting the viability of the technique and that under some circumstances Fe-FeS experimental liquids are nearly quenchable.

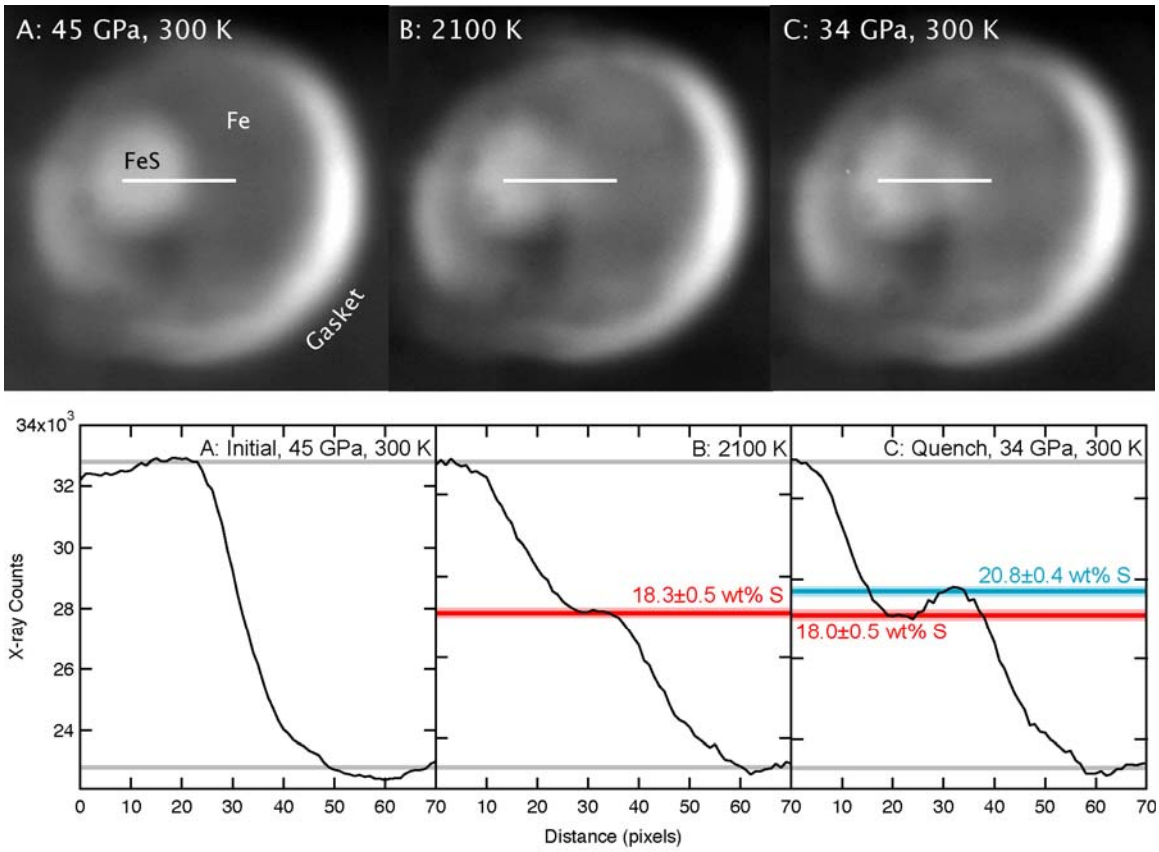


Figure 7 X-radiographic images and absorption profiles of experiment FS-52 which overshot the Fe-FeS eutectic temperature substantially. Fe donut is ~110 μm in diameter. Complex behavior is observed *in situ* to develop during the heating and is preserved in both the quench image and its absorption profile. This behavior would be difficult to interpret were it only observed in a quench image.

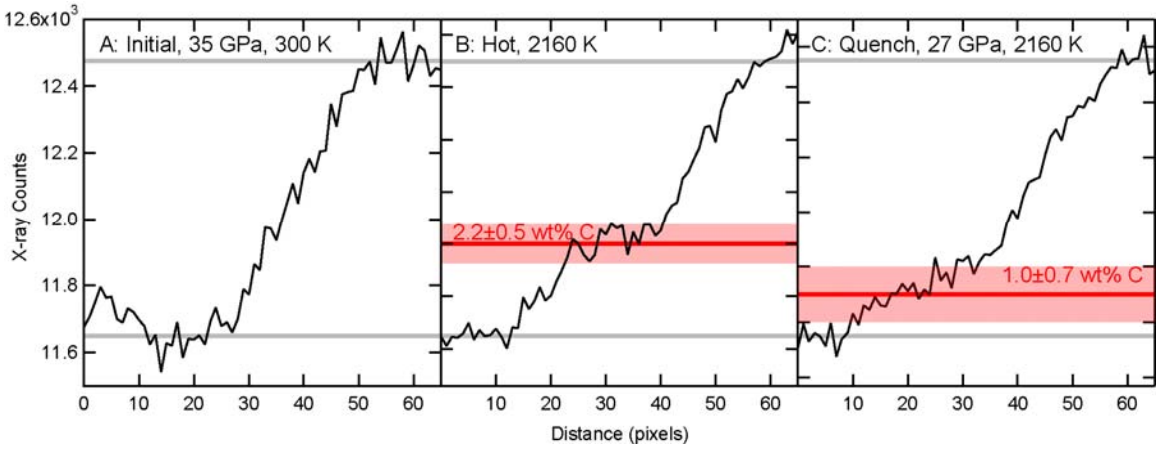


Figure 8 Absorption profiles of experiment FC-45 in which the donut filling was $Fe_3C$. Fe donut is ~110 μm in diameter. There is a clear degradation of the first melting ledge upon quench with the liquid compositional ledge slumping into a ragged slope over an average compositional range that is half the *in situ* value. This unquenchable behavior is frequently encountered in systems Fe-$Fe_3C$ and Fe-FeSi that we report on elsewhere and contrasts with the typical behavior in Fe-FeS which is semiquenchable.

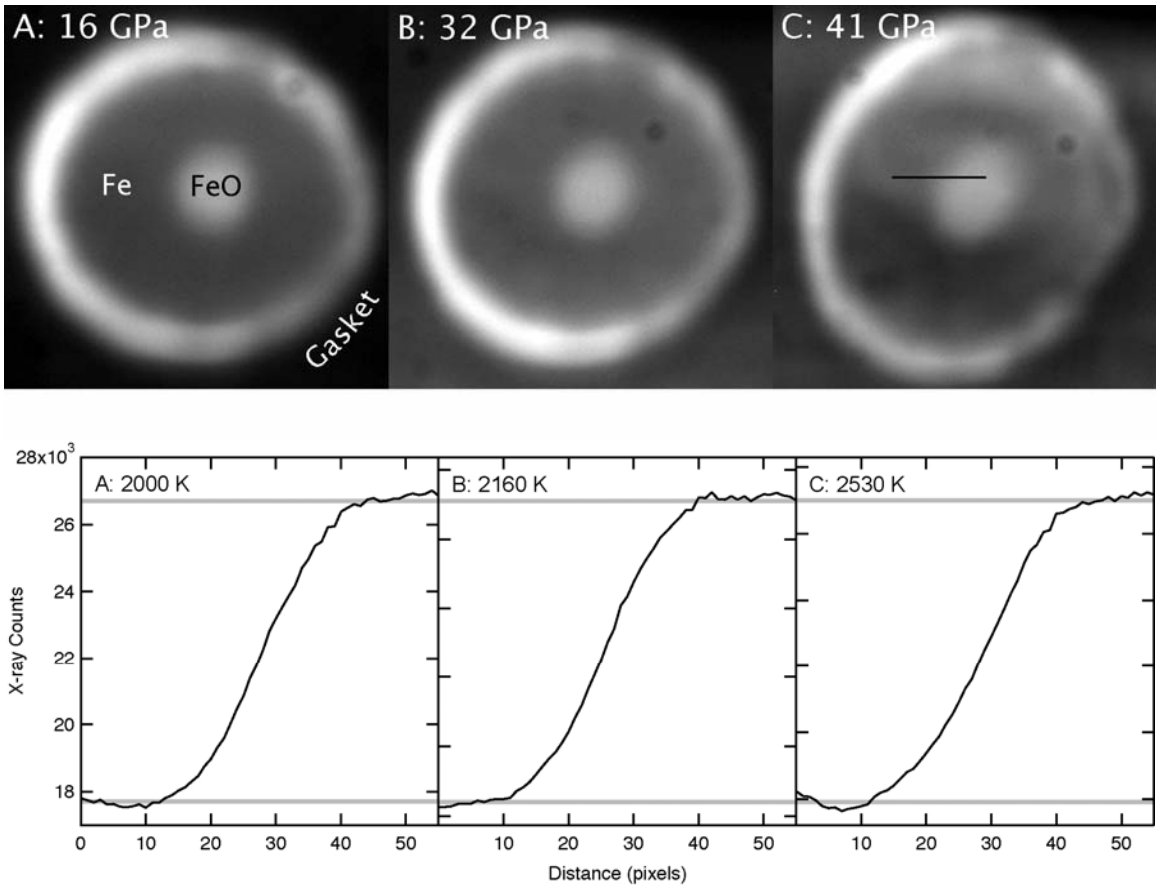


Figure 9 X-radiographic images and absorption profiles in experiment FO-58 in which the donut filling was FeO. Fe donut is ~110 μm in diameter. The images show a sequence of progressing compressions to 41 GPa during which some topographic complexity is introduced to the image by deformation. The absorption profiles (all at initial pressure of 41 GPa which fell to 40 GPa on heating) show no development of a ledge for the first melting even at 2530 K.

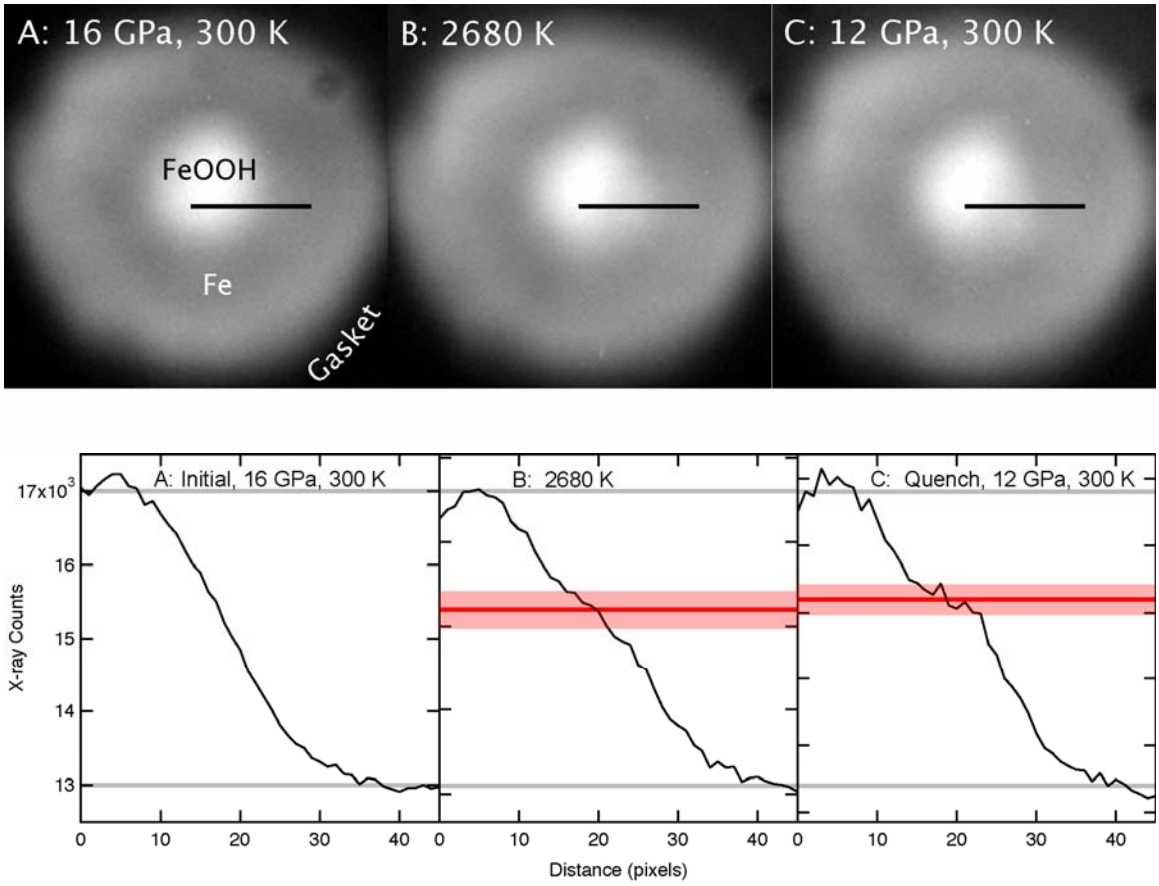


Figure 10 X-radiographic images and absorption profiles for experiment FOH-57 in which the donut filling was FeO(OH). Fe donut is ~110 μm in diameter. A reactive ledge develops on heating - unlike in Fe-FeO experiments. X-ray absorption imaging is not useful for the determination of the reacted liquid composition unless the (OH) enters the liquid without disproportionation, which is currently unknown. Departures from binary behavior cannot be detected with this method. However it is safe to say from the imaging that because both reactants are eroded and the compositional ledge is intermediate to the end members, the reaction is even, not odd, in the chemographic sense.